Journal of Non-Crystalline Solids 592 (2022) 121751

Contents lists available at ScienceDirect

Journal of Non-Crystalline Solids

journal homepage: www.elsevier.com/locate/jnoncrysol

Effect of bond valence sum on the structural modeling of lead borate glass

Masaaki Nagao [a], Shinichi Sakida [b], Yasuhiko Benino [a,*], Tokuro Nanba [a], Atsushi Mukunoki [c], Tamotsu Chiba [c], Takahiro Kikuchi [c], Tomofumi Sakuragi [d], Hitoshi Owada [d]

[a] Graduate School of Environmental and Life Science, Okayama University, 3-1-1 Tsushima-naka, Kita-ku, Okayama 700-8530, Japan
[b] Environmental Management Center, Okayama University, 3-1-1 Tsushima-naka, Kita-ku, Okayama 700-8530, Japan
[c] JGC Japan Corporation, 2-3-1 Minato Mirai, Nishi-ku, Yokohama 220-6001, Japan
[d] Radioactive Waste Management Funding and Research Center, 6-4 Akashicho, Chuo-ku, Tokyo 104-0044, Japan

ARTICLE INFO

Keywords:
Lead borate glass
Reverse Monte Carlo modeling
Bond valence sum
Coordination polyhedron

ABSTRACT

The structural model of 66.7PbO-33.3B_2O_3 glass was constructed using a reverse Monte Carlo (RMC) method, in which bond valence sum (BVS) was added as a constraint condition to suppress formation of unrealistic local structures. Based on the crystal structures, the optimal BVS calculating conditions were determined. As a result, BVS distributions with small deviation were successfully achieved without lowering the reproducibility of other experimental constraints. The geometric asymmetry of PbO_n polyhedra was evaluated from the eccentric distance between Pb and gravity center of oxygen atoms. The average eccentric distance was shorter than that in the lead borate crystals, indicating less asymmetry of PbO_n units in the RMC glass model. The connectivity between BO_n and PbO_n units was investigated. It was consequently concluded that the glass had a different network structure from the crystal with the same composition, which might be due to the different chemical bonding character between the lead borate glasses and crystals.

1. Introduction

Glasses containing PbO have features such as high refractive index, low melting point and radiation shielding ability. Due to these characteristics, lead borate glasses have been used in various applications, and their structure has been investigated [1–7]. Tanabe et al. reported the application of a PbO-ZnO-B_2O_3 glass frit to immobilization of Iodine-129, which is a radionuclide with extremely long half-life and high volatility [1]. It is indispensable to evaluate the long-term nuclide confinement performance of the vitrified materials not only in experiments but also in theoretical simulations. In the simulation of dissolution or leaching process, structural information in the atomic level such as arrangement of the constituents is essential. Regarding the structure of lead borate glass, Akasaka et al. suggested based on X-ray diffraction (XRD) and molecular dynamics (MD) studies that PbO-2B_2O_3 glass has group structures of di-pentaborate and di-triborate, which is different from the PbB_4O_7 crystal with the same composition but a densely-packed rigid structure consisting of three coordinated oxygen [2]. Meera et al. claimed according to Raman spectra that at ~70 mol% PbO, chain-type and ring-type metaborate groups $[B_3O_6]^{3-}$ and 'loose' diborate groups $[B_4O_9]^{6-}$ are present instead of pyroborate $[B_2O_5]^{4-}$ groups [3]. Takaishi et al. reported from XRD analyses that Pb atoms in the glasses with higher PbO content form PbO_3 trigonal pyramids to act as a network former, and in the low-PbO glasses, however, they form PbO_6 octahedra as a network modifier [4]. Hosono et al. concluded from electron spin resonance (ESR) analyses that PbO_n units in 3PbO-B_2O_3 glass have trigonal- or tetragonal-pyramidal structure [5].

Mukunoki et al. have carried out structural analyses of PbO-ZnO-B_2O_3 glasses based on various techniques such as NMR (nuclear magnetic resonance), XAFS (X-ray absorption fine structure), XPS (X-ray photoelectron spectroscopy) spectroscopic methods and X-ray and neutron diffraction methods [6, 7], and they also constructed structural models by using Reverse Monte Carlo (RMC) calculations [7]. In the RMC models, however, even when EXAFS (extended X-ray absorption fine structure) constraints were added, some unrealistic local structures were formed; for example, Pb atoms coordinated by extremely small or large numbers of O atoms, distortion of the polyhedral units, and wide distribution of formal charge of the constituents. The reason why such the unrealistic structures are produced in the RMC models is supposed to be the lack of constraints to minimize the local energy.

The RMC simulation [8] is one of the structural modeling methods, where three-dimensional models for liquids and glasses can be

* benino@okayama-u.ac.jp
E-mail address: benino@okayama-u.ac.jp (Y. Benino).

https://doi.org/10.1016/j.jnoncrysol.2022.121751
Received 18 March 2022; Received in revised form 10 June 2022; Accepted 11 June 2022
Available online 23 June 2022

constructed to reproduce various experimental data (e.g. X-ray diffraction, neutron scattering, NMR, and XAFS). In the RMC modeling, the experimental data used as constraints reflect principally the interatomic distances but no energetic interactions, which may allow the unrealistic local structures. It is expected that Ab-initio calculations are helpful to avoid such the unrealistic structures, and however, it has not yet been implemented in the RMC programs publicly available.

Among the constraints which can be used in the RMC programs, it has been clarified that bond valence sum (BVS) is effective to reproduce chemically reasonable structures [9, 10]. BVS is a simple but sophisticated concept which takes into account interatomic distance and coordination number, and if BVS is estimated correctly, the value should be equal to the ideal ionic charge or formal valence. Therefore, it has also been used widely in the stability evaluation of crystal structures [9, 10]. Sajiki et al. applied BVS constraint to the RMC simulation of Nb_2O_5-0.8H_2O amorphous thin film, and it was revealed that BVS constraint is effective to increase the structural regularity around H atoms with less structural information [11].

Then, in the present study, BVS constraint was also introduced in the RMC calculation to suppress the formation of unrealistic local structures. Structural models of 66.7PbO-33.3B_2O_3 glass were constructed by using the RMCA computer program [12], where sets of experimental information obtained from neutron and X-ray diffraction and ^{11}B MAS NMR measurements were used as the constraints other than the BVS constraint. Furthermore, the reproducibility of structures characteristic of lead borate crystals was evaluated by comparing the local structures around Pb and O atoms against RMC models.

2. Experimental and simulation procedures

2.1. Bond valence sum

BVS of an atom *i*, V_i is given by the following equation [9].

$$V_i = \sum_j s_{ij} = \sum_j \exp\left(\frac{R_0 - R_{ij}}{B}\right) \quad (1)$$

where s_{ij} is the bond valence, that is, the charge transferred between the atoms *i* and *j*, and R_{ij} is the bond length. R_0 and B are the parameters which are characteristic of the pair of atoms.

In the present study, BV parameter sets reported elsewhere [13–15] were used. BVS calculating condition, that is, the upper limit (cutoff) distance for the BV accumulation was examined from the related crystals, where the crystallographic data of 25 crystals containing Pb^{2+} [16–38] and 19 crystals containing B^{3+} [16–32] were collected from the Crystallography Open Database (COD) [39] and the Cambridge Crystallographic Data Center (CCDC) [40]. BVS values of Pb^{2+} and B^{3+} atoms were calculated by changing the cutoff distance, and the appropriate cutoff distance was determined to reach the target BVS values. In the BVS evaluation, the BVS values of anions, not only oxygen but also sulfur and fluorine present in the crystals were also estimated.

2.2. RMC calculation

The structural model for 66.7PbO-33.3B_2O_3 glass was obtained using the RMCA program [12]. As the initial atomic configuration satisfying periodic boundary condition, 6480 atoms (Pb, 1440; B, 1440; O, 3600) were randomly distributed in a cubic cell corresponding to the atomic number densities of 0.06879 Å^{-3}. The constraints based on the experimental facts [7] were (1) neutron scattering structure factor, $S^N(Q)$, (2) X-ray diffraction structure factor, $S^X(Q)$, and (3) the fraction of 4-fold coordinated boron, N_4 of 32% determined by ^{11}B MAS-NMR. In addition to these constraints, BVS constraints were also applied to all the elements, Pb, B, and O to increase their local structural order in the RMC model.

3. Results

3.1. Determination of the optimal BV parameter set

Fig. 1 shows the bond valence of PbO pairs, s_{PbO} and bond valence sum of Pb atoms, V_{Pb} for $Pb_6B_{10}O_{21}$ and $Pb_2B_2O_5$ crystals [30, 31], which have three and six Pb sites. R_0 = 2.032 Å and B = 0.442 Å [15] were used as the parameter set when calculating the bond valence. The continuous curve shows the s_{PbO} in Eq. (1) at the Pb-O distance of R_{PbO}. The vertical bars with different colors indicate s_{PbO} for the respective Pb-O pairs at R_{PbO}. The filled circles with different colors exhibit V_{Pb} of the respective Pb accumulated over R_{PbO}. V_{Pb} tends to increase with increasing R_{PbO}, reaches almost 2.0 at 3.0 - 3.2 Å, and then turned to a gradual increase. A similar trend is also confirmed in other Pb-containing crystals.

Fig. 2 shows the BV and BVS values for the Pb and B sites in various crystals. Figs. 2(a) - 2(c) were obtained from Pb^{2+}-containing crystals [16–38], in which BV and BVS values were calculated from the different BV parameter sets [13–15]. In these figures, a wide distribution of the BVS values is commonly observed at $R_{PbO} \leq 3.2$ Å, and at $R_{PbO} \geq 3.2$ Å, however, the BVS distribution becomes narrower, converging to the nominal valence of +2. In the determination of the appropriate BV parameters which enable to reproduce more-ordered structures, it was considered desirable shorter M-O distance at which V_M reaches its target value and smaller V_M dispersion at the M-O distance where an objective coordination number (Pb: 3 - 6, B: 3, 4) is reproduced, in which longer

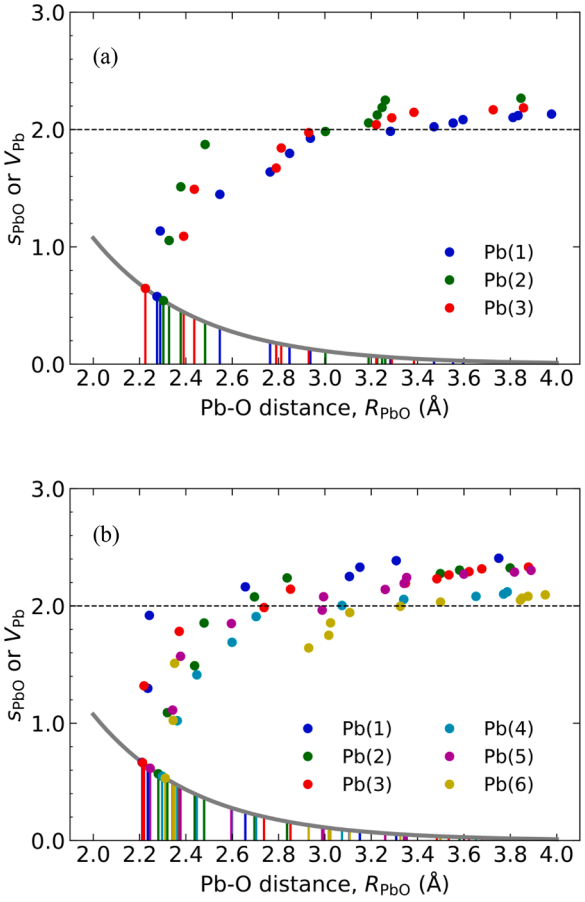

Fig. 1. Bond valence s_{PbO} and bond valence sum V_{Pb} of the Pb sites in (a) $Pb_6B_{10}O_{21}$ and (b) $Pb_2B_2O_5$ crystals. The curve shows s_{PbO} at Pb-O bond distance R_{PbO}, where BV parameters R_0 and B used are 2.032 Å and 0.442 Å, respectively. The vertical bars and filled circles show the s_{PbO} and cumulative V_{Pb} values, respectively, at the distances from each Pb to the respective O atoms.

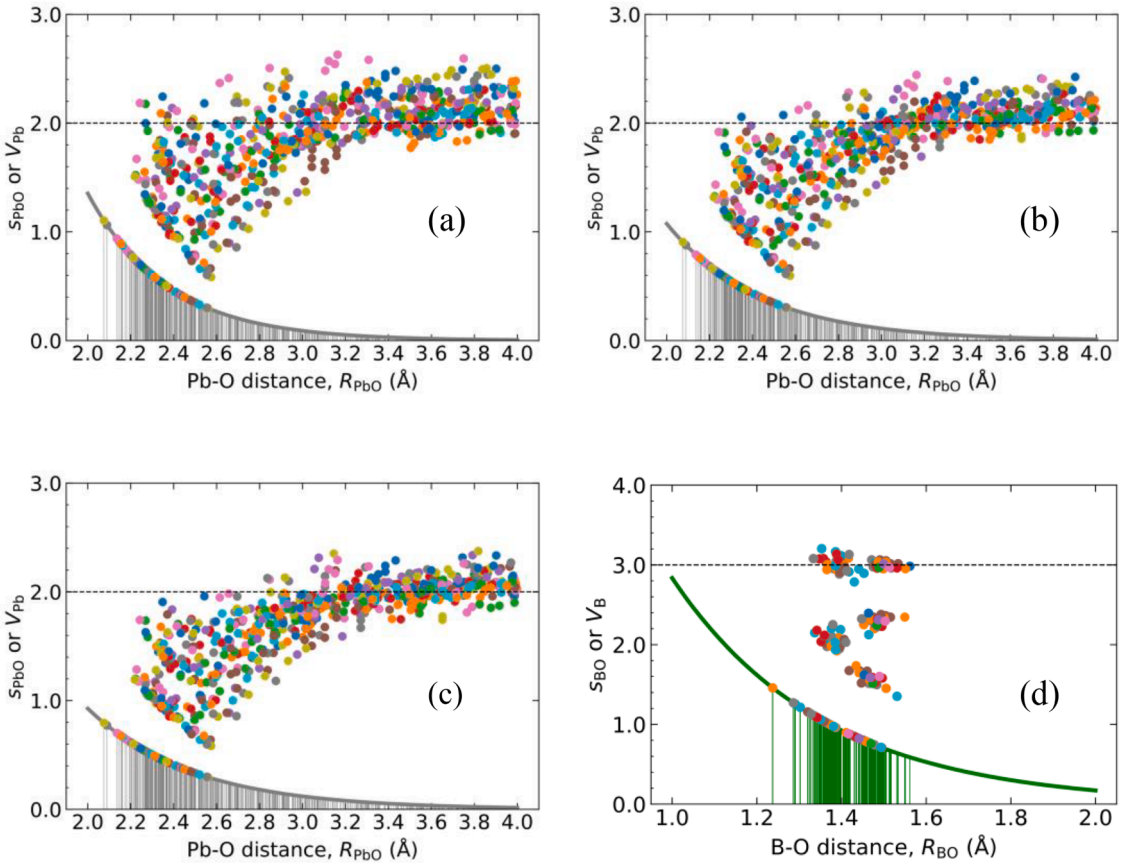

Fig. 2. Bond valence s_{MO} and bond valence sum V_M (M = Pb or B) in the crystals containing Pb^{2+} or B^{3+} calculated from the different BV parameter sets, (a) R_0 = 2.112 Å, B = 0.37 Å, (b) R_0 = 2.032 Å, B = 0.442 Å, (c) R_0 = 1.963 Å, B = 0.49 Å, (d) R_0 = 1.372 Å, B = 0.357 Å. The curve shows s_{MO} at M-O bond distance R_{MO}, and the vertical bars and filled circles show the s_{MO} and cumulative V_M values, respectively, at the distances from each M to the respective O atoms.

limit of the M-O distance will be used as a cutoff distance for the BV accumulation. In Fig. 2(a), the slope of the s_{PbO} curve is largest in the short Pb-O distance region, and V_{Pb} reaches ~2.0 at the shortest R_{PbO}, but the dispersion of V_{Pb} is greatest as compared with the results shown in Figs. 2(b) and 2(c). The V_{Pb} dispersion in Figs. 2(b) and 2(c) is similar, but V_{Pb} seems to reach 2.0 at the different R_{PbO} of ~3.2 Å in Fig. 2(b) and ~3.5 Å in Fig. 2(c), respectively. Then, the BV parameter set, R_0 = 2.032 Å, B = 0.442 Å [15] used in Fig. 2(b) was selected for the BVS calculation in the subsequent RMC simulations, where the cutoff distance of Pb-O pair was determined as 3.2 Å. Fig. 2(d) shows the BV and BVS values for the B sites in 19 crystals [16–32], where a BV parameter set in Ref. 15 was used. V_B reaches 3.0 at R_{BO} ~1.4 Å, at which, however, the coordination number of B is three. Four-coordinated boron atoms in the crystals give the V_B plots at ~1.5 Å in Fig. 2(d), suggesting that cutoff distances longer than 1.4 Å should be used to reproduce BO_4 units. Therefore, the B-O cutoff distance of 1.55 Å and the BV parameter set of R_0 = 1.372 Å, B = 0.357 Å used in Fig. 2(d) were chosen for the BVS constraint. In the RMCA program used, only one cutoff distance can be set as a BVS constraint parameter for an atomic species, and hence the cutoff distance for oxygen was set to 3.2 Å, which is the same as the cutoff distance for Pb.

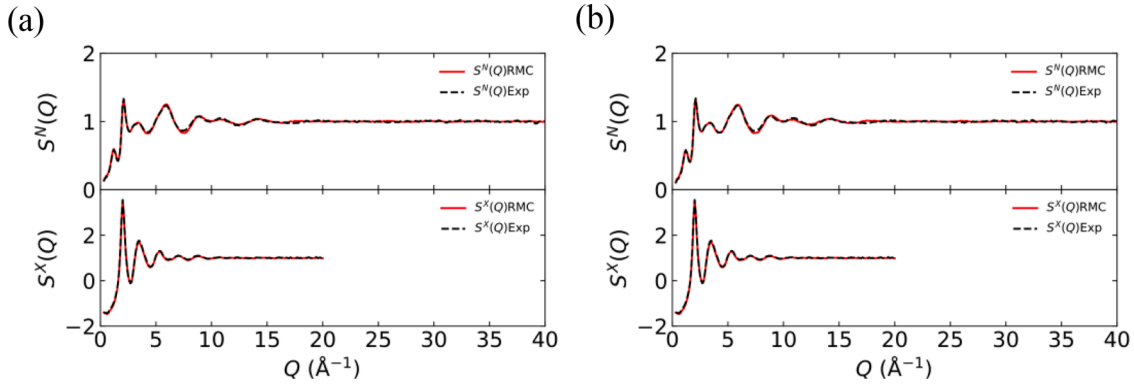

Fig. 3. Structure factors of neutron scattering $S^N(Q)$ and X-ray diffraction $S^X(Q)$ for 66.7PbO-33.3B_2O_3 glass . Red curves: RMC glass models, black dashed curves: experiments. (a) with BVS constraints, (b) without BVS constraints.

3.2. Effects of BVS constraint on the structural reproducibility

By using the optimal BV parameter sets, RMC calculation was performed, and for comparison, the calculation without applying the BVS constraints was also executed. Fig. 3 shows the structure factors of neutron scattering, $S^N(Q)$ and X-ray diffraction, $S^X(Q)$ of 66.7PbO-33.3B_2O_3 glass. Even after applying the BVS constraints, the structure factors of the RMC glass model exhibit good agreement with the experimental ones, and the change in the residual sum of squares χ^2 of structure factors is quite small: χ^2 of $S^N(Q)$ with BVS constraints model $= 2.62 \times 10^3$, without BVS constraint model $= 2.72 \times 10^3$, and χ^2 of $S^X(Q)$ with BVS constraints model $= 4.54 \times 10^3$, without BVS constraint model $= 4.78 \times 10^3$.

As mentioned, the maximum cutoff distance for the BVS constraints is 3.2 Å, and it was hence expected before the RMC calculation that the BVS constraints would not give any effect on the middle to long-range structures in the RMC glass models. As shown in Fig. 3, however, high reproducibility is kept over almost the entire Q region. Fig. 4 shows the partial pair distribution functions, $g_{ij}(r)$. It is recognized that the BVS constraints induce slight change in $g_{ij}(r)$. After applying the BVS constraints, shorter B-O pairs in the first $g_{ij}(r)$ peak increases slightly, and as described later, however, N_4 remains unchanged. Thus, the structural changes in the RMC glass model due to the BVS constraints seem to be very small according to the $S(Q)$ and $g_{ij}(r)$. However, significant changes are found in the local structures around the glass constituents.

Fig. 5 shows the coordination number distributions of Pb and B. As already described, to obtain the target V_{Pb} value of 2.0, it is required to accumulate the s_{PbO} values up to 3.2 Å, which evokes that Pb and O form a Pb-O bond if their distance is less than 3.2 Å. As shown in Fig. 4, however, Pb-O pair gives a first $g_{ij}(r)$ peak at ~2.3 Å, and the longer end of the peak is at around 2.7 Å not 3.2 Å. Another peak with the end at 3.2 Å is not seen in the Pb-O $g_{ij}(r)$ curve so that the number of O atoms around a Pb atom within 2.7 and 3.2 Å was counted and used as a coordination number of Pb. As shown in Fig. 5(a) for the case of 2.7 Å, a narrower distribution for Pb is successfully achieved by applying the BVS constraints, and in Fig. 5(b) for the case of 3.2 Å, however, a narrower distribution is certainly obtained, but the change is not so drastic. Comparing Figs. 5(a) and 5(b), the distribution of Pb coordination number shifts larger side in the longer R_{PbO} of 3.2 Å, which may appear as if the coordination structure has changed. However, it is noteworthy to emphasize that Figs. 5(a) and 5(b) are obtained from the same RMC model, and the only difference is the cutoff distance R_{PbO} for estimating the coordination numbers of Pb. As for the RMC model with the BVS constraint, Fig. 5(a) indicates that 3- and 4-coordinated Pb atoms are predominant in the coordination sphere of 2.7 Å, and Fig. 5(b) also suggests that Pb-O bonds longer that 2.7 Å are present in a non-negligible amount. As for B shown in Fig. 5(c), no change in the distribution is observed. As mentioned, the coordination number constraint was applied even in the RMC calculation without the BVS constraints, and it is, therefore, reasonable to obtain the same coordination number distribution in the case of boron.

Fig. 6 shows the BVS distributions of Pb, B, and O in the RMC glass models. By applying the BVS constraints, the average of BVS values approach the respective target values (Pb: 2.0, B: 3.0, O: 2.0), and at the same time, while the root mean square deviations (RMSD) decrease, which may be suggestive of the increase in the local structural order. The decrease in RMSD of V_{Pb} is significant, and it is also remarkable that the RMSD of V_B without the BVS constraint is large even while the coordination number (fraction of 4-fold coordinated boron) constraint is used in the RMC calculation.

As shown in Fig. 6(b), the BVS distribution for B shows noticeable change with the BVS constraint. As defined in Eq. 1, BVS is calculated using the atomic distance and coordination number (number of an atomic pair). Bond valence s_{ij} is sensitive to the atomic distance R_{ij}, particularly in the shorter distance region, which means that BVS V_i, that is, sum of s_{ij}, changes significantly as a result of changing the atomic distance even when the same coordination number (number of neighboring atom j). As shown in Fig. 5(a), the Pb site with coordination numbers of three and four increases by applying the BVS constraint. As mentioned, it was reported that Pb atoms in high-PbO glasses have three or four neighboring O atoms [4, 5], and it is, therefore, acceptable to form a larger amount of three- and four-coordinated Pb atoms. However, when BV accumulation was quitted at $R_{PbO} = 2.7$ Å as in the case of Fig. 5(a), V_{Pb} did not reach 2.0. It suggests that Pb-O interaction at $R_{PbO} > 2.7$ Å is surely present even for the Pb atoms with apparent coordination numbers of 3 and 4, that is, these Pb atoms also interact with the fifth or sixth oxygen at a distance greater than 2.7 Å to achieve V_{Pb} of 2.0.

Thus, based on these results, it is supposed that the BVS constraint is effective to reproduce highly-ordered geometrical arrangement in the RMC glass model. It should also be mentioned that the Pb site with the coordination number of one disappears after applying the BVS constraint, which suggests that the BVS constraint is also effective to remove unrealistic coordination structures.

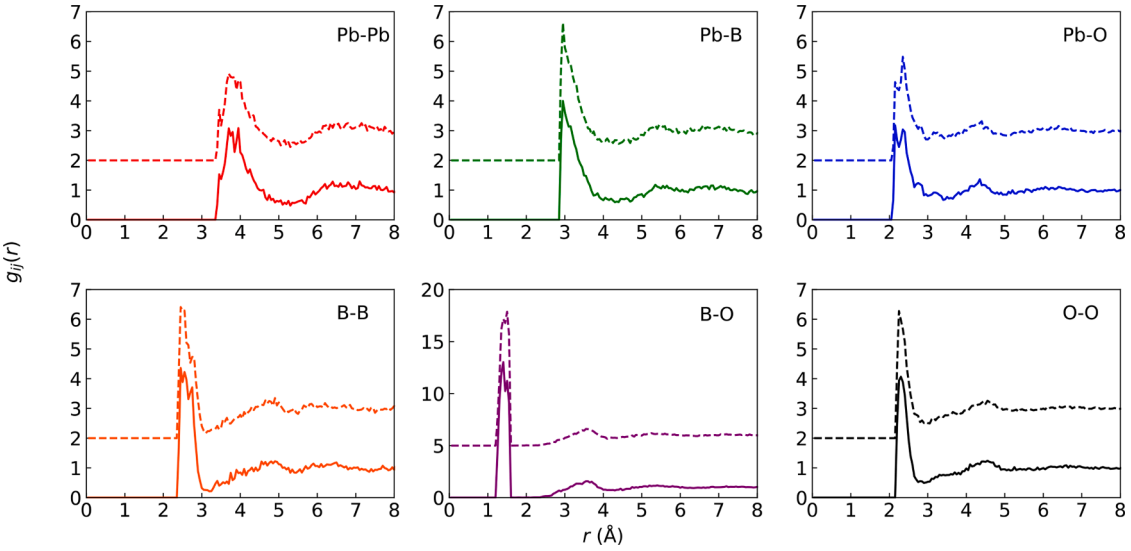

Fig. 4. Partial pair distribution functions $g_{ij}(r)$ of the RMC models for 66.7PbO-33.3B_2O_3 glass. Solid curve: with BVS constraints, dotted curve: without BVS constraints.

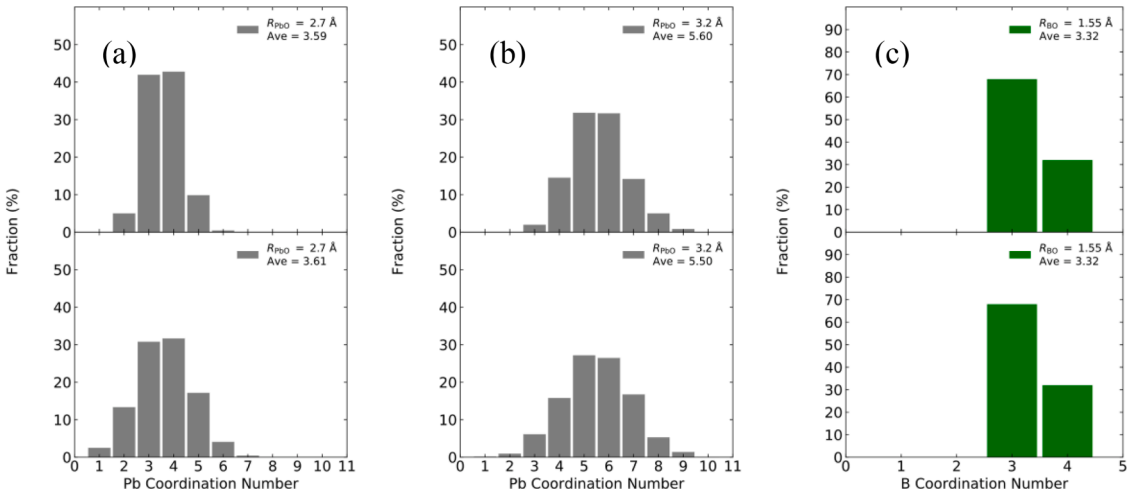

Fig. 5. Coordination number distributions in the RMC models for 66.7PbO-33.3B_2O_3 glass (upper: with BVS constraints, lower: without BVS constraints). Coordination numbers were obtained within the Pb- or B-centered spheres with the radius R_{MO}. (a) Pb-O in the coordination sphere of 2.7 Å, (b) Pb-O in the coordination sphere of 3.2 Å, (c) B-O in the coordination sphere of 1.55 Å.

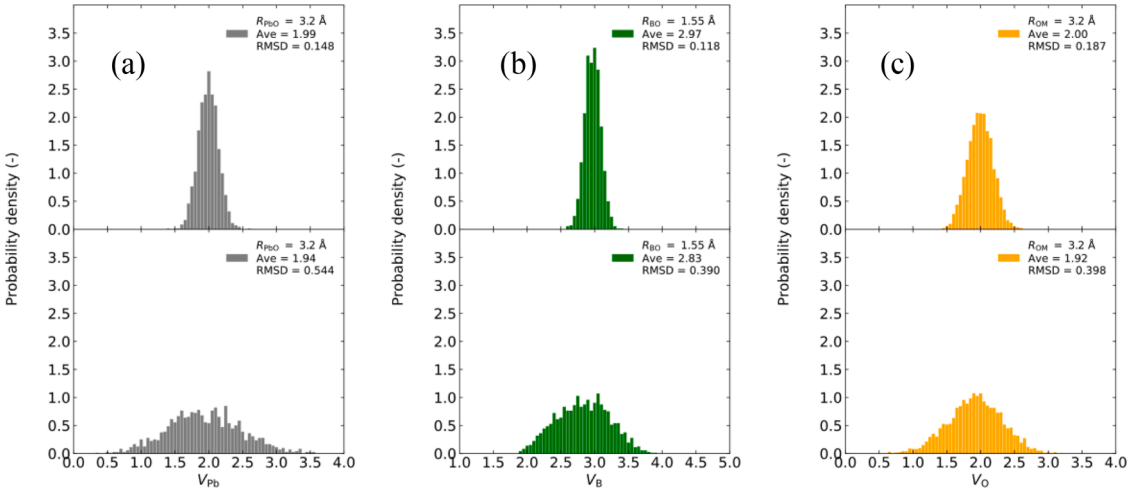

Fig. 6. BVS distributions of (a) Pb, (b) B, (c) O atoms in the RMC models for 66.7PbO-33.3B_2O_3 glass. Upper: with BVS constraints, lower: without BVS constraints. The width of each bar is 0.05, and the bar length (probability density) is normalized so that the total bar area becomes 1.0. R_{PbO}, R_{BO}, and R_{OM} mean the upper limit distance for the bond valence accumulation. Ave and RMSD indicate the average and the root mean square deviation of BVS, respectively.

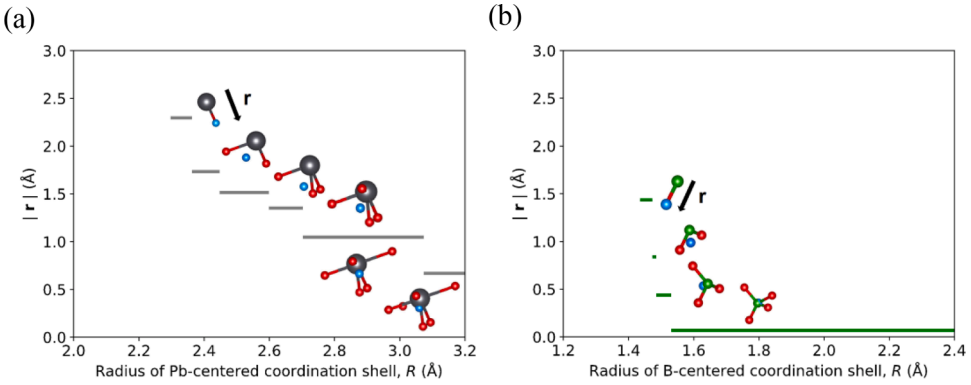

Fig. 7. Eccentric distance | **r** | between the center of gravity of oxygen atoms, O_{CG} and (a) Pb or (b) B in $Pb_2B_2O_5$ crystal. O_{CG} was determined for the oxygen atoms within the Pb- or B-centered coordination shell with the radius R. In the coordination models, Pb, B, O, and O_{CG} are drawn by black, green, red, and blue balls, respectively.

4. Discussion

4.1. Symmetry of polyhedral units

As shown in Figs. 5 and 6, from the viewpoint of coordination number, the unrealistic structures around Pb with very small coordination numbers seemed to have been removed by introducing the BVS constraint, and a narrow BVS distribution has been successfully achieved. Pb^{2+} ions possess $6s^2$ lone pair electrons, and due to the electrostatic repulsion between electron pairs, PbO_3 and PbO_4 polyhedra have distorted shapes of trigonal pyramid, trigonal bipyramid, and square pyramid. Then, the symmetry of PbO_n and BO_n units was examined based on the geometric arrangement.

As for the geometric symmetry of an MO_n polyhedron, the eccentric distance $|\mathbf{r}|$ between the center of gravity of oxygen atoms, O_{CG} and the cation M was evaluated. As shown in Fig. 7, an MO_n unit within the M-centered coordination shell with the radius R is extracted, and the M-O_{CG} distance at R is calculated to obtain $|\mathbf{r}|$. Fig. 8 shows the eccentric distance $|\mathbf{r}|$ for the PbO_n and BO_n units in the RMC glass model obtained with the BVS constraints and lead borate crystals. A similar result was obtained in the RMC glass model without applying the BVS constraints. It is commonly observed that $|\mathbf{r}|$ decreases with increasing the radius of Pb- or B-centered coordination shell, R. Regarding the BO_n polyhedra in the lead borate crystals, as shown in Fig. 8(b), $|\mathbf{r}|$ becomes almost zero, when the last ligand oxygen, that is, third or fourth neighboring oxygen enters the coordination shell. In the case of the BO_n polyhedra in the RMC glass model, a similar trend is confirmed, but $|\mathbf{r}|$ is widely distributed near zero, indicating that BO_3 and BO_4 units are not in regular triangular and tetrahedral shapes and have larger distortion. On the other hand, as for the PbO_n polyhedra shown in Fig. 8(a), the $|\mathbf{r}|$ distribution even in the crystals is less convergent than that of the BO_n polyhedra, and at $R = 3.2$ Å, most of the PbO_n polyhedra in the crystals take the $|\mathbf{r}|$ values larger than 0.5 Å, indicating the asymmetric shape of the PbO_n polyhedra. It is also notable that the $|\mathbf{r}|$ values of PbO_n polyhedra in the RMC glass model decrease faster than those in the crystals with expanding the coordination sphere, that is, with the increase in R. It is consequently suggested that the PbO_n polyhedra in the RMC glass model have higher symmetry than those in the crystals, and even with introducing the BVS constraint, it is difficult to fully reproduce the asymmetric arrangement characteristic of the PbO_n polyhedra. If the actual lead borate glass consists of PbO_n polyhedra with the completely same shapes as the lead borate crystals, additional constraints, such as O-Pb-O bond angle restriction, should be used in the RMC calculations, or structural optimization of PbO_n polyhedra based on Ab-initio calculations should be applied to the RMC glass model. EXAFS constraint is also applicable to the RMC calculation, and in the case of glass, the information obtained from Pb-EXAFS spectrum is restricted to the Pb-O bond length and coordination number. Therefore, it is hardly expected to reproduce the same geometry of PbO_n units as the lead borate crystals with the EXAFS constraint.

4.2. Local structure around oxygen atoms and connectivity of BO_n and PbO_n units

In the previous section, the slight symmetry differences in the PbO_n and BO_n polyhedra between the RMC glass model and the lead borate crystals were confirmed. In this section, local structures around oxygen atoms, that is, connectivity of the PbO_n and BO_n polyhedra were examined, and the reproducibility of the structural characteristics in the crystals to the RMC glass model was evaluated.

First, the structural characteristics in the lead borate crystals were investigated by classifying the oxygen atoms by the type of surrounding boron and lead atoms, where lead borate crystals with different composition ($PbO\text{-}2B_2O_3$, $6PbO\text{-}5B_2O_3$, $2PbO\text{-}B_2O_3$, and $4PbO\text{-}B_2O_3$) [29–32] were selected. Fig. 9 shows the bond valence s_{OM} (M = B3, B4, and Pb) and the cumulative bond valence sum V_O for the oxygen sites in these crystals, where B3 and B4 indicate 3-coordinated and 4-coordinated boron atoms, respectively. The BV values (s_{OB3}, s_{OB4}, and s_{OPb}) for each oxygen site were calculated for the boron and lead atoms within the oxygen-centered coordination shell with a radius of 3.2 Å, and they are shown by the vertical bars. In these crystals, the following characteristic oxygen atoms are present, that is, tri-cluster oxygen surrounded by three B4 (Fig. 9(a), O-index: 0-3), non-bridging oxygen (NBO) bonded to one B4 (Fig. 9(b), O-index: 19-20 and Fig. 9(c), O-index: 10-13), and isolated oxygen surrounded only by Pb (Fig. 9(c), O-index: 14 and Fig. 9(d), O-index: 22-27), where Pb^{2+} is assumed as a network modifier. It is generally understood that the oxygen atoms mentioned above are absent or rarely found in typical alkali borate glasses. It is also noteworthy that even for the bridging oxygen (BO) bonded to two B, V_O reaches 2.0 due to the additional interaction with Pb.

Next, the RMC model of $66.7PbO\text{-}33.3\ B_2O_3$ glass was analyzed using the same procedure. Fig. 10 shows the result with the BVS constraints, and almost the same result was obtained without using the BVS constraints. A similar trend found in the lead borate crystals is also reproduced in the RMC glass model. Even for the typical bridging oxygen bonded to two boron atoms, the contribution of lead atoms is not negligible to attain V_O of 2.0. The RMC glass model has the same composition as $2PbO\text{-}B_2O_3$ crystal (Fig. 9(c)), and in the RMC glass model, however, the oxygen atoms, such as tri-cluster oxygen and B3-O-B3 bridging oxygen which are not present in the crystal, are formed. Table 1 shows the classification of oxygen in the RMC glass model and the crystals. The fraction of bridging oxygen, including tri-cluster oxygen, is ~41% in the RMC glass model and ~53% in $2PbO\text{-}B_2O_3$ crystal with the same composition as the glass. As for non-bridging oxygen, a larger amount of NBO (B-O-Pb) is produced in the RMC glass model as compared with the crystal. Thus, network connectivity seems to be

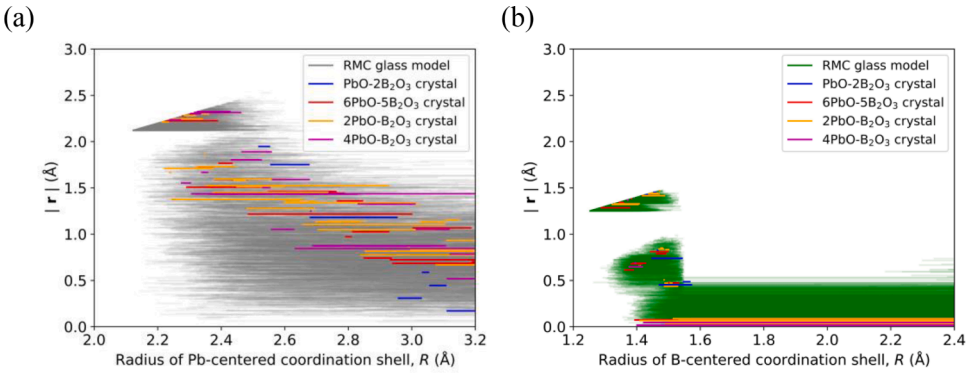

Fig. 8. Eccentric distance $|\mathbf{r}|$ between the center of gravity of oxygen atoms, O_{CG} and (a) Pb or (b) B in the RMC glass model obtained with the BVS constraints and lead borate crystals. O_{CG} was determined for the oxygen atoms within the Pb- or B-centered coordination shell with the radius R.

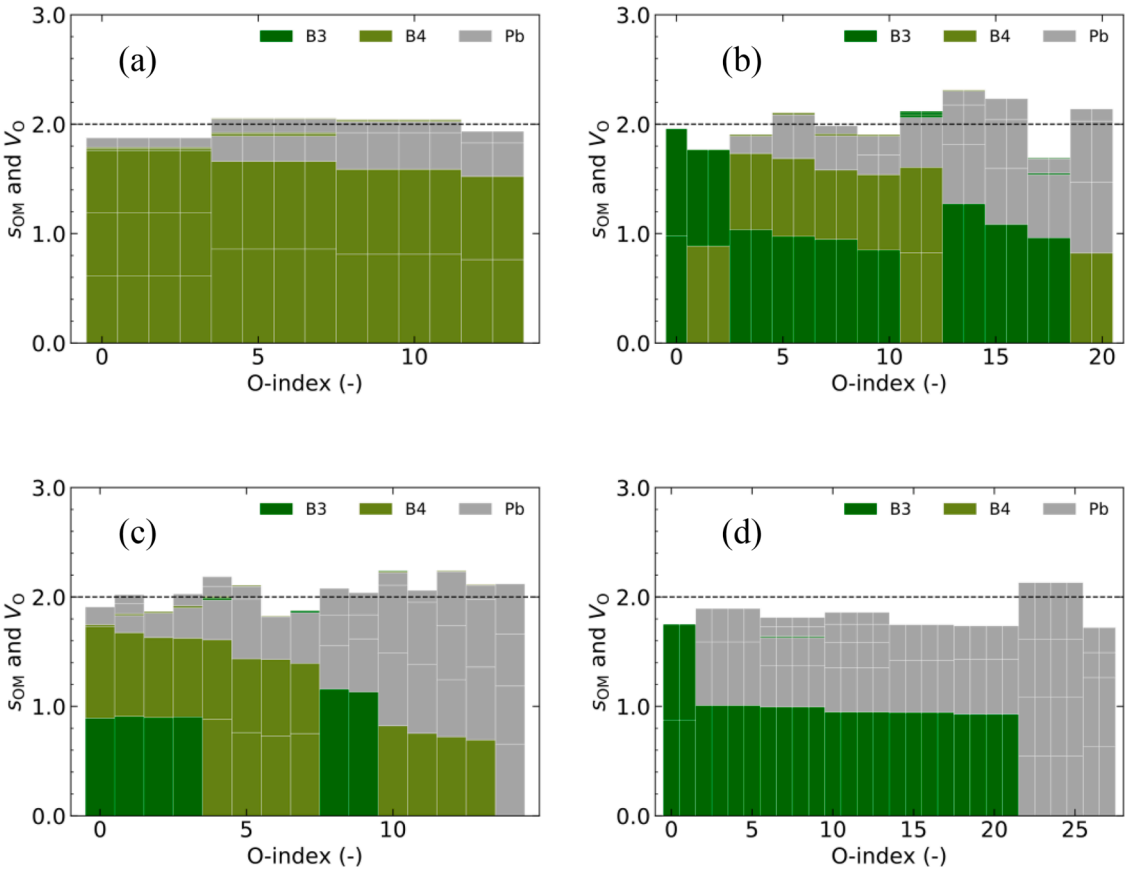

Fig. 9. Bond valence s_{OM} (M = B3, B4, and Pb) and cumulative bond valence sum V_O of the O sites in the lead borate crystals of (a) PbO-$2B_2O_3$, (b) 6PbO-$5B_2O_3$, (c) 2PbO-B_2O_3, and (d) 4PbO-B_2O_3, where B3 and B4 indicate 3-coordinated and 4-coordinated boron atoms, respectively. The O sites are sorted by Σs_{OB} accumulated over the neighboring B3 and B4 atoms.

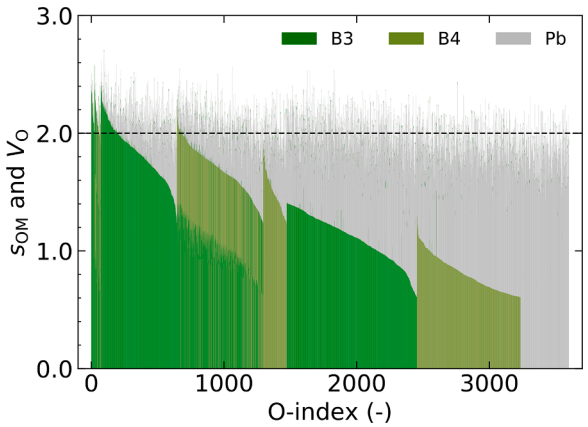

Fig. 10. Bond valence s_{OM} (M = B3, B4, and Pb) and cumulative bond valence sum V_O of the O sites in the RMC model of 66.7PbO-33.3B_2O_3 glass obtained with the BVS constraints, where B3 and B4 indicate 3-coordinated and 4-coordinated boron atoms, respectively. The O sites are sorted by Σs_{OB} accumulated over the neighboring B3 and B4 atoms

different between the RMC glass model and the crystal with the same composition.

Density and N_4 value of the 66.7PbO-33.3B_2O_3 glass are experimentally measured as 6.65 g/cm^3 and 32%, and those of the 2PbO-B_2O_3 crystal are 7.16 g/cm^3 and 67%, respectively, suggesting that the glass has a sparser packing structure than the crystal, which is also consistent with the formation of a larger amount of NBO in the RMC model. It is consequently acceptable that the lead borate glass has different network

Table 1
Fraction (%) of oxygen atoms in the RMC model of 66.7PbO-33.3B_2O_3 glass and the related crystals of PbO-$2B_2O_3$, 6PbO-$5B_2O_3$, 2PbO-B_2O_3, and 4PbO-B_2O_3.

	RMC glass model		crystal		
	66.7PbO-33.3B2O3	PbO-2B2O3	6PbO-5B2O3	2PbO-B2O3	4PbO-B2O3
O≡	2.0	28.6	0.0	0.0	0.0
B3-O-B3	15.9	0.0	4.8	0.0	7.1
B3-O-B4	18.1	0.0	47.6	26.7	0.0
B4-O-B4	4.9	71.4	9.5	26.7	0.0
B3-O$^-$	27.3	0.0	28.6	13.3	71.4
B4-O$^-$	21.7	0.0	9.5	26.7	0.0
O^{2-}	10.1	0.0	0.0	6.7	21.4

connectivity from the crystal. Such a different network structure is also found in PbO-$2B_2O_3$ glass and crystal [2].

It is commonly recognized that NBO has higher polarizability than BO, because more electrons are localized on NBO. In the lead borate glass, oxygen in B-O-Pb bonds is regarded as NBO, and hence oxygen atoms in PbO_3 and PbO_4 units in the RMC model should have a relatively higher proportion of NBO. Then, it is supposed in the RMC model that electrostatic repulsion between the oxygen atoms in PbO_3 and PbO_4 units is greater, resulting in wider O-Pb-O bond angles and shorter eccentric distances of PbO_3 and PbO_4 units. The structure of a material is ruled by its chemical bonding character, and it is supposed that change in the chemical bonding character leads to the formation of different chemical species, such as B3, B4, BO, NBO, and so on. The structural

difference between the lead borate glass and crystal may be essential, which originates from the different chemical bonding character.

If so, even when the interatomic potential obtained from the lead borate crystals is used to construct the structural models, it may not be possible to reproduce the structures present in the actual lead borate glasses. The structural difference as seen in Fig. 8(a), that is, the faster decrease in the eccentric distance of PbO_n units in the RMC glass model, may be essential in the lead borate glasses. It was supposed from Fig. 8 (a) that further RMC constraint is required to reproduce the PbO_n units with correct structures, but the structures that actually exist in the lead borate glass may have been already reproduced in the present RMC glass model.

5. Conclusion

The BVS constraint was applied to the RMC calculation for 66.7PbO-33.3B_2O_3 glass to suppress the formation of unrealistic coordination structures of PbO_n units. The optimal BV parameter set and the appropriate cutoff distance were determined based on a large number of crystals containing Pb, B, and O atoms. After applying BVS constraints, the narrower distributions in BVS and coordination number of lead atoms in the RMC glass model were successfully attained without degrading the reproducibility of experimental facts, such as the structure factors and the fraction of 4-fold coordinated boron atoms. The eccentric distance | **r** | was investigated to evaluate the geometric symmetry of PbO_n and BO_n units in the RMC glass model. BO_n units in the lead borate crystals had | **r** | values close to zero, and those in the RMC glass model showed widely distributed | **r** | values near zero. As for the PbO_n polyhedra, the | **r** | values did not converge to zero for both the RMC glass model and the crystals, and a faster decrease in the | **r** | values with expanding the coordination sphere was observed in the RMC glass model, denoting that PbO_n units in the RMC glass model had higher symmetry than those in the lead borate crystals. The local structure around oxygen in the RMC glass model was evaluated to examine the connectivity of PbO_n and BO_n units. The oxygen atoms characteristic of the lead borate crystals, such as tri-cluster oxygen, B4-O-Pb, and Pb-O-Pb, were also reproduced in the RMC glass model. However, the relative contents of oxygen atoms with different coordination structures disagreed between the RMC glass model and 2PbO-B_2O_3 crystal with the same composition, supporting the difference in network connectivity between the actual lead borate glass and crystal. In order to elucidate the cause of the structural difference, it might be necessary to understand deeply the nature of chemical bonds in lead borate glasses.

CRediT authorship contribution statement

Masaaki Nagao: Conceptualization, Methodology, Software, Writing – original draft. **Shinichi Sakida:** Investigation, Resources. **Yasuhiko Benino:** Conceptualization, Methodology, Validation, Formal analysis. **Tokuro Nanba:** Writing – review & editing, Supervision. **Atsushi Mukunoki:** Investigation, Resources. **Tamotsu Chiba:** Investigation, Resources. **Takahiro Kikuchi:** Investigation, Resources. **Tomofumi Sakuragi:** Project administration. **Hitoshi Owada:** Project administration, Funding acquisition.

Declaration of Competing interest

Hitoshi Owada reports financial support was provided by Agency for Natural Resources and Energy.

Acknowledgements

This study was carried out under a contract with the Ministry of Economy, Trade and Industry (METI) as part of its R&D supporting program titled " Advancement of Processing and Disposal Technique for the Geological disposal of TRU Waste (FY2019 and FY2020) (JPJ007597)".

References

[1] H. Tanabe, T. Sakuragi, K. Yamaguchi, T. Sato, H. Owada, Development of New Waste Forms to Immobilize Iodine-129 Released from a Spent Fuel Reprocessing Plant, Adv. Sci. Technol. 73 (2010) 158–170, https://doi.org/10.4028/www.scientific.net/AST.73.158.

[2] Y. Akasaka, I. Yasui, T. Nanba, Network structure of RO•2B_2O_3 glasses, Phys. Chem. Glasses 34 (1993) 232–237.

[3] B.N. Meera, A.K. Sood, N. Chandrabhas, J. Ramakrishna, Raman study of lead borate glasses, J. Non-Cryst. Solids 126 (1990) 224–230, https://doi.org/10.1016/0022-3093(90)90823-5.

[4] T. Takaishi, J. Jin, T. Uchino, T. Yoko, Structural Study of PbO–B_2O_3 Glasses by X-ray Diffraction and ^{11}B MAS NMR Techniques, J. Am. Chem. Soc. 83 (2000) 2543–2548, https://doi.org/10.1111/j.1151-2916.2000.tb01588.x.

[5] H. Hosono, H. Kawazoe, T. Kanazawa, Coordination of Pb^{2+} in Oxide Glasses Determined by ESR and Properties of Binary Lead Glasses, Yogyo-Kyokai-Shi 90 (1982) 544–551, https://doi.org/10.2109/jcersj1950.90.1045_544.

[6] A. Mukunoki, T. Chiba, Y. Suzuki, K. Yamaguchi, T. Sakuragi, T. Nanba, Further Development of Iodine Immobilization Technique by Low Temperature Vitrification With $BiPbO_2I$, in: Proceedings of the ASME 2009 12th International Conference on Environmental Remediation and Radioactive Waste Management 1, 2009, pp. 329–334, https://doi.org/10.1115/ICEM2009-16268.

[7] A. Mukunoki, T. Chiba, Y. Benino, T. Sakuragi, Microscopic structural analysis of lead borate-based glass, Prog. Nucl. Energy. 91 (2016) 339–344, https://doi.org/10.1016/j.pnucene.2016.05.008.

[8] R.L. McGreevy, L. Pusztai, Reverse Monte Carlo Simulation: A New Technique for the Determination of Disordered Structures, Mol. Simulat. 1 (1988) 359–367, https://doi.org/10.1080/08927028808080958.

[9] I.D. Brown, The Chemical Bond in Inorganic Chemistry, Oxford University Press, Oxford, 2002.

[10] I.D. Brown, Recent Developments in the Methods and Applications of the Bond Valence Model, Chem. Rev. 109 (2009) 6858–6919, https://doi.org/10.1021/cr900053k.

[11] G. Sajiki, Y. Benino, C. Oki, K. Ohara, H. Okano, T. Nanba, Structural analyses and reverse Monte Carlo modeling of niobium oxide amorphous film prepared by sputtering method, J. Ceram. Soc. Japan 125 (2017) 760–765, https://doi.org/10.2109/jcersj2.17053.

[12] M.A. Howe, R.L. McGreevy, J.D. Wicks, RMCA—A general purpose Reverse Monte Carlo Code, 1993. Manual.

[13] I.D. Brown, D. Altermatt, Bond-Valence Parameters Obtained from a Systematic Analysis of the Inorganic Crystal Structure Database, Acta Cryst B41 (1985) 244–247, https://doi.org/10.1107/S0108768185002063.

[14] S.V. Krivovichev, I.D. Brown, Are the compressive effects of encapsulation an artifact of the bond valence parameters? Z. Kristallogr. 216 (2001) 245–247, https://doi.org/10.1524/zkri.216.5.245.20378.

[15] O.C. Gagné, F.C. Hawthorne, Comprehensive derivation of bond-valence parameters for ion pairs involving oxygen, Acta Cryst B71 (2015) 562–578, https://doi.org/10.1107/S2052520615016297.

[16] H. Park, J. Barbier, R.P. Hammond, Crystal structure and polymorphism of $PbAlBO_4$, Solid State Sci 5 (2003) 565–571, https://doi.org/10.1016/S1293-2558(03)00056-6.

[17] L. Dong, S. Pan, Y. Wang, H. Yu, X. Dong, S. Han, M. Zhang, Special $^1_\infty[OPb_2]$ Chains and $^1_\infty[O_2Pb_3]$ Ribbons Based on OPb_4 Anion-Centered Tetrahedra in $Pb_2(O_4Pb_8)(BO_3)_3Br_3$ and $Pb_2(O_8Pb_{12})(BO_3)_2Br_6$, Inorg. Chem 52 (2013) 11377–11384, https://doi.org/10.1021/ic401655h.

[18] X.-A. Chen, Y.-H. Zhao, X.-A. Chang, L. Zhang, H.-P. Xue, Lead zinc borate, $PbZn_2(BO_3)_2$, Acta Cryst C62 (2006) i11–i12, https://doi.org/10.1107/S0108270105040709.

[19] Y. Wang, S. Pan, S. Huang, L. Dong, M. Zhang, S. Han, X. Wang, Structural insights for the design of new borate–phosphates: synthesis, crystal structure and optical properties of $Pb_4O(BO_3)(PO_4)$ and $Bi_4O_3(BO_3)(PO_4)$, Dalton Trans 43 (2014) 12886–12893, https://doi.org/10.1039/C4DT01199F.

[20] B. Aurivillius, The Crystal-Structure of a Basic Lead Borate Sulfate, $Pb_6O_2(BO_3)_2SO_4$, Chem Scr 22 (1983) 168–170.

[21] H. Behm, Hexalead chloride triorthoborate oxide, $Pb_4O[Pb_2(BO_3)_3Cl]$, Acta Cryst C39 (1983) 1317–1319, https://doi.org/10.1107/S0108270183008367.

[22] J.-L. Song, C.-L. Hu, X. Xu, F. Kong, J.-G. Mao, $Pb_2B_3O_{5.5}(OH)_2$ and $[Pb_3(B_3O_7)](NO_3)$: Facile Syntheses of New Lead(II) Borates by Simply Changing the pH Values of the Reaction Systems, Inorg. Chem 52 (2013) 8979–8986, https://doi.org/10.1021/ic401175r.

[23] S. Pan, B. Watkins, J.P. Smit, M.R. Marvel, I. Saratovsky, K.R. Poeppelmeier, Structure and Magnetic Properties of $Pb_2Cu_3B_4O_{11}$: a New Copper Borate Featuring $[Cu_3O_8]^{10-}$ Units, Inorg. Chem 46 (2007) 3851–3855, https://doi.org/10.1021/ic0614824.

[24] O.V. Yakubovich, N.N. Mochenova, O.V. Dimitrova, W. Massa, Reinvestigation of the $Pb_2[B_5O_9]Br$ structure based on single-crystal data, Acta Cryst E60 (2004) i127–i130, https://doi.org/10.1107/S1600536804023232.

[25] M. Mutailipu, M. Zhang, B. Zhang, Z. Yang, S. Pan, The first lead fluorooxoborate PbB_5O_8F: achieving the coexistence of large birefringence and deep-ultraviolet cut-off edge, Chem. Commun. 54 (2018) 6308–6311, https://doi.org/10.1039/C8CC02694G.

[26] Y.-Z. Huang, L.-M. Wu, X.-T. Wu, L.-H. Li, L. Chen, Y.-F. Zhang, $Pb_2B_5O_9I$: An Iodide Borate with Strong Second Harmonic Generation, J. Am. Chem. Soc. 132 (2010) 12788–12789, https://doi.org/10.1021/ja106066k.
[27] H. Yu, H. Wu, S. Pan, B. Zhang, L. Dong, S. Hanabc, Z. Yang, $Pb_4Zn_2B_{10}O_{21}$: a congruently melting lead zinc borate with a novel $[B_{10}O_{24}]$ anionic group and an interesting $[Pb_4O_{12}]_\infty$ chain, New J. Chem. 38 (2014) 285–291, https://doi.org/10.1039/C3NJ00893B.
[28] H. Park, R. Lam, J.E. Greedan, J. Barbier, Synthesis, Crystal Structure, Crystal Chemistry, and Magnetic Properties of $PbMBO_4$ (M = Cr, Mn, Fe): A New Structure Type Exhibiting One-Dimensional Magnetism, Chem. Mater 15 (2003) 1703–1712, https://doi.org/10.1021/cm0217452.
[29] D.L. Corker, A.M. Glazer, Structure and optical non-linearity of $PbO.2B_2O_3$, Acta Cryst B52 (1996) 260–265, https://doi.org/10.1107/S0108768195013310.
[30] J. Krogh-Moe, P.S. Wold-Hansen, The crystal structure of hexalead pentaborate, $6PbO.5B_2O_3$, Acta Cryst B29 (1973) 2242–2246, https://doi.org/10.1107/S0567740873006412.
[31] F. Zhang, F. Zhang, B.-H. Lei, Z. Yang, S. Pan, Synthesis, Characterization, and Theoretical Studies of $(Pb_4O)Pb_2B_6O_{14}$: A New Lead(II) Borate with Isolated Oxygen-Centered Pb_4O Tetrahedra and Large Second Harmonic Generation Response, J. Phys. Chem. C 23 (2016) 12757–12764, https://doi.org/10.1021/acs.jpcc.6b03862, 120.
[32] H. Yu, S. Pan, H. Wu, W. Zhao, F. Zhang, H. Li, Z. Yang, A new congruent-melting oxyborate, $Pb_4O(BO_3)_2$ with optimally aligned BO_3 triangles adopting layered-type arrangement, J. Mater. Chem. 22 (2012) 2105–2110, https://doi.org/10.1039/C1JM14590H.
[33] H.H. Grube, Die Struktur des $(PbO)_3(B_2O_3)_5(H_2O)_2$, Fortschritte der Mineralogie, Beiheft 59 (1981) 58–59.
[34] S. Giraud, J-P. Wignacourt, M. Drache, G. Nowogrocki, H. Steinfink, The Stereochemical Effect of $6s^2$ Lone-Pair Electrons: The Crystal Structure of a New Lead Bismuth Oxyphosphate $Pb_4BiO_4PO_4$, J. Solid State Chem. 142 (1999) 80–88, https://doi.org/10.1006/jssc.1998.7988.
[35] L.S. Dent Glasser, R.A. Howie, R.M. Smart, The structure of lead 'orthosilicate', $2PbO.SiO_2$, Acta Cryst B37 (1981) 303–306, https://doi.org/10.1107/S0567740881002902.
[36] D.F. Mullica, H.O. Perkins, D.A. Grossie, L.A. Boatner, B.C. Sales, Structure of dichromate-type lead pyrophosphate, $Pb_2P_2O_7$, J. Solid State Chem. 62 (1986) 371–376, https://doi.org/10.1016/0022-4596(86)90252-5.
[37] R.J. Angel, U. Bismayer, W.G. Marshall, Local and long-range order in ferroelastic lead phosphate at high pressure, Acta Cryst B60 (2004) 1–9, https://doi.org/10.1107/S0108768103026582.
[38] M.T. Averbuch-Pouchot, A. Durif, Structure of lead tetrapolyphosphate, Acta Cryst C43 (1987) 631–632, https://doi.org/10.1107/S0108270187094745.
[39] S. Gražulis, A. Daškevič, A. Merkys, D. Chateigner, L. Lutterotti, M. Quirós, N. R. Serebryanaya, P. Moeck, R.T. Downs, Armel Le Bail, Crystallography Open Database (COD): an open-access collection of crystal structures and platform for world-wide collaboration, Nucleic Acids Research D1 (2012) D420–D427, https://doi.org/10.1093/nar/gkr900.
[40] F.H. Allen, The Cambridge Structural Database: a quarter of a million crystal structures and rising, Acta Cryst B58 (2002) 380–388, https://doi.org/10.1107/S0108768102003890.